European Journal of Radiology 81 (2012) e647–e652

Contents lists available at SciVerse ScienceDirect

European Journal of Radiology

journal homepage: www.elsevier.com/locate/ejrad

Analysis of perfusion defects by causes other than acute pulmonary thromboembolism on contrast-enhanced dual-energy CT in consecutive 537 patients

Bo Hyun Kim [1], Joon Beom Seo *, Eun Jin Chae [1], Hyun Joo Lee [1], Hye Jeon Hwang [1], Chaehun Lim [1]

Department of Radiology and Research Institute of Radiology, University of Ulsan College of Medicine, Asan Medical Center, 388-1, Poongnap-dong, Songpa-gu, Seoul 138-736, Republic of Korea

ARTICLE INFO

Article history:
Received 10 November 2011
Received in revised form 12 January 2012
Accepted 17 January 2012

Keywords:
Dual-energy CT
Perfusion map
Lung diseases
Pulmonary thromboembolism
Perfusion defect

ABSTRACT

Objective: To assess causes, incidence and patterns of perfusion defects (PDs) on dual-energy perfusion CT angiography (DECTA) in clinically suspected acute pulmonary thromboembolisms (PTE).
Materials and methods: Consecutive 537 patients who underwent DECTA for suspicion of PTE were retrospectively reviewed. After excluding patients with possible PTE or unsatisfactory perfusion map quality, 299 patients with 1697 lobes were included. The DECTA (Somatom Definition, Siemens) was performed at 140 kV and 80 kV. Color-coded perfusion images were obtained with a lung PBV application of the workstation software (Syngo Dual Energy). The presence, incidence, three patterns of PDs (wedge-shaped, heterogeneous, and regionally homogeneous), pulmonary diseases, and the matchedness between the PD and the disease extent were studied.
Results: 315 of 1697 lobes (18.6%) in 156 of 299 patients (81.3%) showed PDs. Among them, 51 (3%), 257 (15.1%), and 7 (0.4%) lobes had PDs due to vascular, nonvascular, and unidentifiable causes, respectively. Vascular causes include: pulmonary arterial (PA) hypertension (0.7%), extrinsic occlusion of PA by fibrosis (0.6%), PA hypoplasia (0.6%), vasculitis (0.5%), cancer mass compressing PA, venous occlusion, AVM, and pulmonary angiosarcoma. Most of PDs were wedge-shaped and well-matched. Nonvascular causes include: mosaic attenuation (4.1%), emphysema (3.2%), interstitial fibrosis (1.6%), bronchitis (1.4%), GGO (1.2%), cellular bronchiolitis (1%), bronchiectasis, airway obstruction, compensaroty lung hyperinflation, air trapping, cor-pulmonale, bronchopneumonia, physiologic decreased ventilation, and segmental bronchial atresia. Most of PDs showed heterogeneous pattern and were not matched.
Conclusions: Various vascular and nonvascular diseases cause PDs on DECTA. Each disease shows different pattern of PD depending on pathophysiology and physiologic compensation.
© 2012 Elsevier Ireland Ltd. All rights reserved.

1. Introduction

The introduction of dual-energy CT and its unique material-specific imaging ability has made possible the assessment of pulmonary parenchymal perfusion status [1–3]. Although the perfusion map used in the dual-energy CT is actually an "iodine map" that only reflects the static distribution of the iodine in the lung parenchyma at a certain point of time, its potential for intuitive pulmonary perfusion assessment is worth the attention. The major advantage of dual-energy perfusion CT angiography is its ability to visualize perfusion abnormality in pulmonary thromboembolisms [4], in that sharply delineated linear and wedge-shaped perfusion defects are related to pulmonary thromboembolism [5–10]. However, due to various physiologic and pathologic conditions that can lead to decreased pulmonary perfusion, direct application of pulmonary perfusion maps to the diagnosis of pulmonary thromboembolism is somewhat restricted in real clinical practice [11–13]. Nevertheless, there have been only a few reports on causes of perfusion decrease [14–17] and their patterns [15], necessitating the systematic evaluation of the causes and patterns of perfusion defects on dual-energy perfusion CT. We assessed various causes of perfusion defects, along with their incidence and typical pattern on dual-energy perfusion CT in patients clinically suspected of having acute pulmonary thromboembolisms.

Abbreviations: CT, computed tomography; MPR, multi-planar reconstruction; MIP, maximal intensity projection; HU, hounsfield unit; GGO, ground glass opacity; AVM, arteriovenous malformation; PA, pulmonary artery.

* Corresponding author. Tel.: +82 2 3010 4383/4400; fax: +82 2 476 4719.
E-mail addresses: blackgura@hanmail.net (B.H. Kim), seojb@amc.seoul.kr, joonbeom.seo@gmail.com (J.B. Seo), ejinchae@hotmail.com (E.J. Chae), wberry_hj@yahoo.co.kr (H.J. Lee), umttette@hanmail.net (H.J. Hwang), leon7777@gmail.com (C. Lim).
[1] Tel.: +82 2 3010 4388; fax: +82 2 476 4719.

0720-048X/$ – see front matter © 2012 Elsevier Ireland Ltd. All rights reserved.
doi:10.1016/j.ejrad.2012.01.026

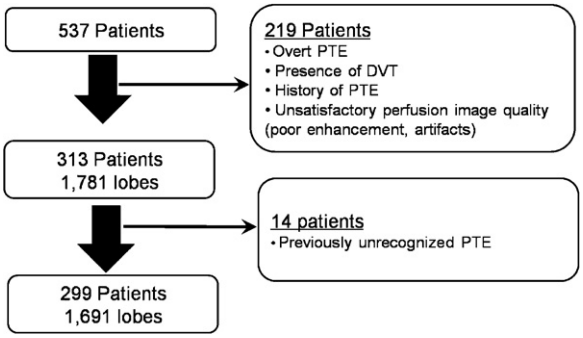

Fig. 1. Patient selection process.

2. Material and methods

2.1. Patient population

We retrospectively assessed 537 consecutive patients who underwent dual-energy pulmonary CT angiography due to clinical suspicion of acute pulmonary thromboembolism from February 2008 to February 2009. To exclude patients with possible pulmonary thromboembolism, we excluded: (a) patients with overt pulmonary thromboembolism on conventional imaging; (b) patients with evidence of deep vein thrombosis of the lower extremities on duplex sonography; (c) patients with a history of pulmonary thromboembolism; (d) patients with unsatisfactory perfusion map quality, primarily due to poor enhancement and/or artifacts; this particular group included perfusion maps with diffusely decreased enhancement in the whole lung; and (e) patients with atelectasis or artifacts accounting for more than 30% of the lobar area. Each lung was considered to have 6 lobes. After applying the exclusion criteria, we had 313 patients (142 males, 171 females; mean age, 62.3 years) with 1781 lobes (six lobes had been resected previously). During the study, we incidentally identified 14 patients with small pulmonary thromboembolisms that had been missed on conventional imaging; after excluding these patients, we had 299 patients with 1697 lobes. An outline of the patient selection process is shown in Fig. 1. This study was approved by our hospital's institutional review board, which waived the requirement for patient informed consent due to the retrospective design of this study.

2.2. Scan and contrast injection protocol

All patients underwent pulmonary CT angiography on a dual-source CT scanner (Somatom Definition scanner, Siemens Healthcare). Each scan was performed with a 512×512 matrix, 14 mm × 1.2 mm collimation, 50 mAs (effective) at 140 kV and 210 mAs (effective) at 80 kV, pitch of 0.5, and gantry rotation time of 0.33 s. Images from the lung apex to the costophrenic angles were acquired in a single breath-hold in the craniocaudal direction. A power injector was used to administer 100 mL of iodine contrast material (iopromide, Ultravist 370, Bayer Schering Pharma) at a rate of 3.5 mL/s, with a fixed scan delay of 20 s.

2.3. Perfusion image generation

Two simultaneous helical scans were acquired with two tubes of 140 and 80 kV. The data from each tube were collected at the two independent tubes (A and B). Data from the 80-kV, 140-kV, and weighted average images were transferred to a workstation (MultiModality Workplace, Siemens Healthcare). Weighted average images of approximately 120 kV were automatically generated from the 140- and 80-kV images, with a weighting factor of 1:4 (140:80 kV). This weighted average image was used for pulmonary CT angiography. A color-coded iodine image was obtained with the lung PBV application of the workstation software (Syngo Dual Energy) based on the material decomposition theory. The application class was designed for iodine extraction, with material parameters of −1000 HU for air at 80 kV, −1,000 HU for air at 140 kV, 60 HU for soft tissue at 80 kV, 54 HU for soft tissue at 140 kV, 2 for relative contrast enhancement, −960 HU for minimum value, −300 HU for maximum value, and 4 for range. A color-coded iodine image was used as the perfusion image. The color-coded iodine map can be superimposed on conventional gray-scale images, and the settings can be adjusted to display any range of blended images, from gray-scale only to iodine maps only.

Of the two detectors, the larger detector (detector A) covered a scan field of view (FOV) (50 cm), while the smaller detector (B system) covered a central FOV (26 cm).

2.4. Image analysis

Images were analyzed by three readers in consensus, using a dedicated workstation and software. Each lung was regarded as having six lobes, including the lingular division. For each lobe, the presence of perfusion defect was evaluated, as was the presence of pulmonary vascular and/or parenchymal pathologies on thin-section 120-kV images. For the latter, the readers were able to adjust settings from default lung-window to mediastinal settings. If necessary, MPR or MIP images were also used. If there were more than two pathologies in one lobe, only the dominant disease which occupies larger part of the lobe was recorded in consensus. Readers calculated the incidence of all perfusion defects in all lobes and in lobes affected by specific diseases. After reviewing the 120-kV images, readers estimated the extent of the disease, and then assessed whether the extent of perfusion defect was correspondent to that of the disease. A mismatch was considered to be present when the region of the defect was within the estimated area of the disease but was smaller in size. Matched perfusion decrease was considered when the area of perfusion abnormality showed no size discrepancy to the estimated area of the disease. Any perfusion defect without a demonstrable pathology was regarded as an unexplained perfusion defect. Readers also assessed the pattern of perfusion defect and categorized it into three classes according to its morphology: (a) wedge-shaped; (b) heterogeneous perfusion defect with intervening areas of preserved perfusion; and (c) regionally distributed diffuse perfusion decrease without intervening areas of preserved perfusion (Fig. 2).

3. Results

We found that 315 of the 1697 lobes (18.6%) in 156 of 299 patients (81.3%) showed perfusion defects. When we classified them into three broad pathological categories, we found that 51 (3%), 257 (15.1%), and 7 (0.4%) had defects due to vascular causes, nonvascular causes, and unidentifiable causes, respectively.

3.1. Vascular causes

Of the vascular causes, pulmonary arterial hypertension was the most common pathologic condition. Some other relatively common causes included fibrosing inflammation compressing the pulmonary artery (Fig. 3), pulmonary arterial hypo/aplasia, and vasculitis. Most of these perfusion defects were wedge-shaped, except in cases due to pulmonary arterial hypoplasia/aplasia, which were heterogeneous.

Overall, physical compression of the pulmonary artery would result in a higher incidence of well-matched perfusion defect. However, the specific shape of it varied greatly, according to factors

Download English Version:

https://daneshyari.com/en/article/6244540

Download Persian Version:

https://daneshyari.com/article/6244540

Daneshyari.com